Int. J. Heat Mass Transfer. Vol. 34, No. 8, pp. 2123–2132, 1991
Printed in Great Britain

0017–9310/91 $3.00+0.00

Theoretical and experimental heat and mass transfer in highly porous media

KUM-BAE LEE
Korea Institute of Energy and Resources, 71-2 Jang-dong, Yousung-ku, Daejeon, Korea

and

JOHN R. HOWELL
Center for Energy Studies and Department of Mechanical Engineering, The University of Texas at Austin, Austin, TX 78712, U.S.A.

(*Received* 27 *March* 1990 *and in final form* 12 *October* 1990)

Abstract—The heat and mass transfer coefficients around the porous medium put on the flat plate at a distance from the leading edge of the flat plate are calculated numerically for two-dimensional laminar flows. To verify the analytical model developed and invoke the heat/mass transfer analogy, an experiment is carried out by the naphthalene sublimation technique for the case of negligible radiation field. From the effects of the wake, the Sherwood number is maximum around the region where the porous medium is attached. The theoretical results correspond well with the experimental results at small Darcy number. Permeability of ceramic blocks used for experiment is also measured and the Forchheimer equation is applicable in our measurement range.

1. INTRODUCTION

An understanding of the heat and mass transfer characteristics of porous media is important for many applications in science and engineering. There are numerous practical situations in which flow passes partly through and partly around a porous body. Common examples are flow over the Earth's surface in the presence of obstructions such as trees, grains, flow over high porosity insulations, and flow for some industrial drying and cooling processes.

Several workers have studied the behavior of wind well inside and above a prototype forest [1, 2]; others modeled a forest or crop for wind tunnel measurements [3, 4].

For forced convection flows, it has been shown that for a Reynolds number based on particle or pore size larger than unity, a velocity square term ($|U|u_i$) to account for porous inertia effects must be added [5]. For higher velocities, many researchers have modified Darcy's law by an addition of convective inertia terms ($u_j\partial u_i/\partial x_j$), porous inertia terms ($|U|u_i$) or viscous terms ($\mu_e\partial^2 u_i/\partial x_j^2$) [6]. The equation with all of the three terms added approaches the theory of the porous medium (simple Darcy's law) as the permeability K decreases, and it goes to the standard Navier–Stokes equation for a fluid as K increases; consequently the analysis connects the two theories.

The idealized model used in the present numerical analysis is shown in Fig. 1, where the two-dimensional medium is assumed to extend to infinity in both directions. One region is a high porosity layer bounded by an impermeable layer on the bottom surface. The upper surface is bounded by a free stream region. An imposed flow is specified at the leading edge of the two-region system.

The energy equations were solved numerically to see the effects of radiative transfer and the results are presented in terms of the heat transfer coefficients and temperatures.

To verify the analytical model developed, an experiment was carried out by the naphthalene sublimation technique for the case of negligible radiation, which has been used by several researchers [7, 8] to obtain mass transport results. Permeability of ceramic blocks used for experiment was also measured.

By using the analogy between heat and mass transfer, the Sherwood number presented here may be converted to the Nusselt number as in the non-porous region if the analogy relations in the porous region are verified from the experimental measurements.

2. THEORETICAL ANALYSIS

The conservation equations of a porous medium, which is regarded as homogeneous and isotropic, were derived in terms of the superficial (Darcian) velocity within the porous medium using a control volume [9].

Porous region.

$$\frac{\partial u}{\partial x}+\frac{\partial v}{\partial y}=0 \tag{1}$$

NOMENCLATURE

b	back-scattered fraction factor
C	concentration
D	mass diffusion coefficient
Da	Darcy number, K/H^2
e_b	black body emissive power, σT^4
F	parameter
H	height of porous medium
h_m	convection mass transfer coefficient
K	permeability of porous medium
k	thermal conductivity
l	upstream length
$\dot{m}$	mass transfer rate
N	convection–radiation flux parameter
Nu	Nusselt number
p	pressure
p_{nw}	naphthalene vapor pressure on the wall
Pe	Peclet number
Pr	Prandtl number
Q	dimensionless radiative heat flux, $q/\sigma T_\infty^4$
q	radiative heat flux
$\bar{R}$	universal gas constant
Re	Reynolds number, $u_\infty H/\nu$
Sc	Schmidt number, ν/D
Sh	Sherwood number
T	temperature
u, v	x- and y-direction velocities, respectively
x, y	x- and y-coordinate.

Greek symbols

ε	porosity
ε_w	wall emissivity
μ	dynamic viscosity
ρ	fluid density or naphthalene vapor density
σ_a	absorption coefficient
σ_e	extinction coefficient
σ_s	scattering coefficient
τ	optical thickness, $\sigma_e H$
ϕ_w	dimensionless wall temperature, T_w/T_∞
ω	scattering albedo, σ_s/σ_e.

Subscripts

e	effective
f	fluid
i, j	tensor notation
m	mass transfer
n	function of Nusselt number
p	porous
r	radiative
s	source or function of Sherwood number
w	wall
∞	free stream.

Superscripts

+, −	positive and negative y-direction, respectively
*	dimensionless.

$$\frac{\rho}{\varepsilon^2}\left(u\frac{\partial u}{\partial x}+v\frac{\partial u}{\partial y}\right)=-\frac{\mathrm{d}p}{\mathrm{d}x}-\frac{\mu}{K}u-\frac{\rho F}{\sqrt{K}}|U|u+\frac{\mu_e}{\varepsilon}\nabla^2 u \tag{2}$$

$$\frac{\rho}{\varepsilon^2}\left(u\frac{\partial v}{\partial x}+v\frac{\partial v}{\partial y}\right)=-\frac{\mathrm{d}p}{\mathrm{d}y}-\frac{\mu}{K}v-\frac{\rho F}{\sqrt{K}}|U|v+\frac{\mu_e}{\varepsilon}\nabla^2 v \tag{3}$$

$$\rho c_p\left(u\frac{\partial T}{\partial x}+v\frac{\partial T}{\partial y}\right)=k_e\nabla^2 T-\nabla q_r \tag{4}$$

$$u\frac{\partial C}{\partial x}+v\frac{\partial C}{\partial y}=D_e\nabla^2 C \tag{5}$$

where

$$|U|=(u^2+v^2)^{1/2}$$

$$k_e=\varepsilon k_f+(1-\varepsilon)k_p$$

$$D_e=\varepsilon D.$$

Models for the effective viscosity μ_e of the porous medium are needed. It has been found that taking $\mu_e \approx \mu$ in Brinkman's extension provides good agreement with experimental data [10] and is adopted in the present work. From the Ergun equation [11] the value of F is $1.75/\sqrt{(150\varepsilon^3)}$ and is adopted in the present work.

The conservation equations outside the porous medium are easily derived from the equations that apply within the porous medium by setting $\varepsilon \to 1$ and $K \to \infty$.

The temperature gradient in the x-direction is assumed to be small compared with that in the y-direction, so that $q_r(x) \ll q_r(y)$. Thus the radiative flux is simply expressed as a one-dimensional approximation

$$q_r(y)=q^+(y)-q^-(y). \tag{6}$$

The two-flux model is expressed as

$$\frac{\mathrm{d}q^+}{\mathrm{d}y}=-2\sigma_a q^+-2\sigma_s b q^++2\sigma_a e_b+2\sigma_s b q^- \tag{7}$$

$$-\frac{\mathrm{d}q^-}{\mathrm{d}y}=-2\sigma_a q^--2\sigma_s b q^-+2\sigma_a e_b+2\sigma_s b q^+. \tag{8}$$

The solid boundary and matrix are assumed diffuse and gray. It is also assumed that the fluid itself is

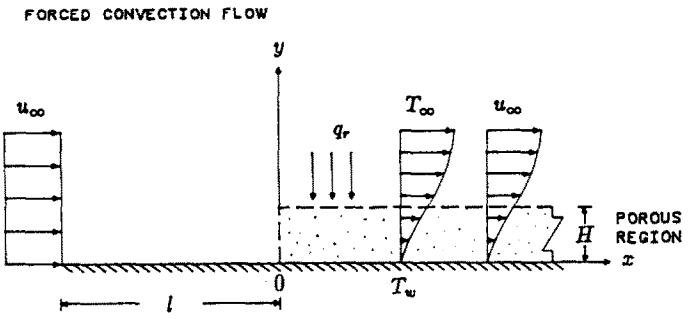

FIG. 1. Schematic of the porous medium at the system boundary with net radiation to the porous medium.

transparent whereas the porous materials emit, absorb, and scatter radiation. The coupled ordinary differential equations describing the radiative transfer in the porous medium are split into two second-order differential equations which are coupled through the boundary conditions. These equations can be solved by the method of variation of parameters.

The dimensionless terms for conservation equations, boundary conditions, two-flux solutions, etc., are not described here because of space limitations. For more detailed solution processes, see ref. [9].

2.1. *Boundary conditions*

The velocity and pressure profiles upstream ($x = -l$) of the porous medium are free stream values. A given boundary layer velocity profile is required at the starting point of the porous medium ($x = 0$), and the distance from the far upstream point (where the velocity distribution is flat) to the start of the porous medium must be specified. The u-velocity profile at the starting point ($x = 0$) is described by a parabolic profile.

With known u-velocity profile and upstream distance, the v-velocity profile and pressure profile are determined from the assumptions that the v-velocity increases linearly from the starting point to the porous medium, and pressure is equal to the free stream pressure over the porous medium. We assume that the temperature has a similar profile to the velocity, and the concentration has a hyperbolic profile. No slip is allowed on the plane surface ($y = 0$). The pressure boundary condition is determined from the y-momentum equation on the plane surface. The temperature and concentration given on the plane surface are assumed constant with x.

At a large value of y, the boundary layer properties match the free stream values. The pressure is assumed to be at the free stream pressure everywhere outside the porous medium.

Far downstream from the starting point, the boundary conditions are unknown. Thus we assume that no more changes occur, that is, the first derivatives are all assumed to be zero.

At the porous/fluid interface ($y = H$), we must have continuity of superficial velocity, normal stress, temperature, heat flux, concentration, and mass flux.

For two-flux model solutions, the source flux is assumed constant outside the porous medium. At the wall, the outgoing energy is emitted plus reflected energy.

2.2. *Method of solution*

The dimensionless governing equations were solved numerically using the finite difference method with associated boundary conditions. The numerical calculations began at the leading edge of the porous medium and proceeded in the streamwise direction to far downstream. The conservation equations were solved using the Thomas algorithm and the pressure equation derived by the x- and y-momentum equations is elliptic and was solved using the successive overrelaxation method (SOR).

The dimensionless parameter, $Nu(x)$, termed the modified Nusselt number, provides a measure of the convection, conduction, plus radiation heat transfer occurring at the surface

$$|Nu| = -\left.\frac{\partial T^*}{\partial y^*}\right|_{y^*=0} + \frac{Pe_c}{N} Q_r|_{y^*=0}. \tag{9}$$

The Nusselt number consists of two components; the first term on the right-hand side of equation (9) is due to convection plus conduction whereas the second term is due to thermal radiation.

The dimensionless parameter, $Sh(x)$, termed the Sherwood number, provides a measure of the convection mass transfer occurring at the surface

$$|Sh| = \frac{h_m H}{D_e} = -\left.\frac{\partial C^*}{\partial y^*}\right|_{y^*=0}. \tag{10}$$

2.3. *Results*

To see the effects of radiative heat transfer, the energy equation was solved numerically and the results are presented in terms of the heat transfer coefficients and temperatures.

Figures 2–5 show the heat transfer coefficients with the effect of radiative transfer included ($Q_s = 0 \sim 3$), using $Re = 500$, $Da = 0.005$, $\varepsilon = 0.98$, $\omega = 0.5$,

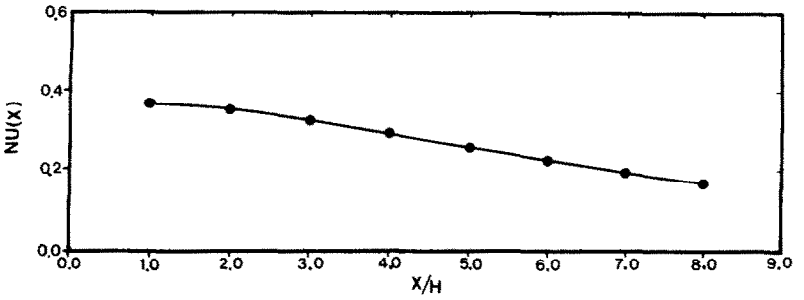

FIG. 2. Nusselt number ($Q_s = 0$).

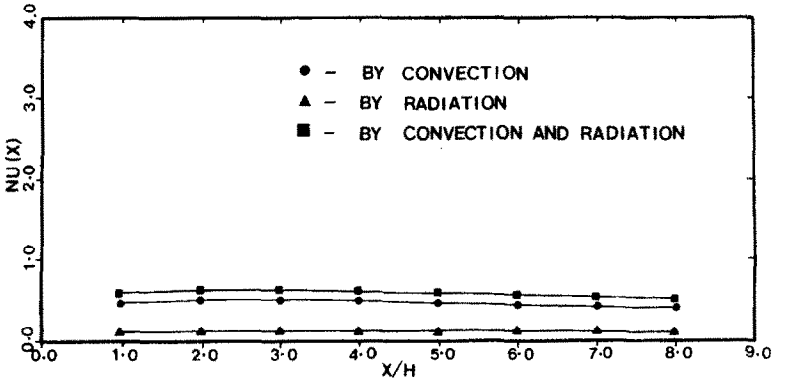

FIG. 3. Nusselt number ($Q_s = 1$).

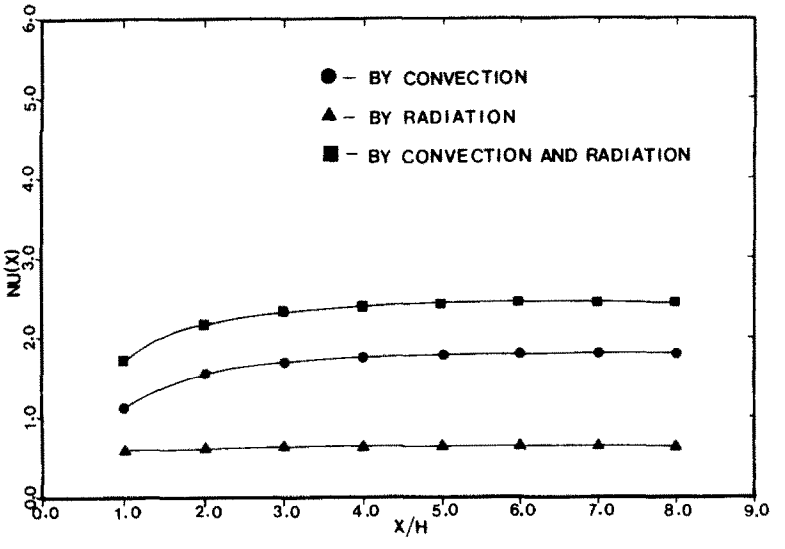

FIG. 4. Nusselt number ($Q_s = 2$).

$b = 0.5$, $\varepsilon_w = 0.5$, $\phi_w = 0.95$ and $\tau = 1$. Figure 2 shows only the convection heat transfer coefficient in the absence of radiative transfer. The rate of decrease is almost constant along the x-direction.

Figures 3–5 show the individual heat transfer coefficients calculated for convection, radiation, and convection plus radiation (here called the total heat transfer coefficient). The total heat transfer coefficient in Fig. 3 increases at first with the effects of the radiation, but past the location of $x/H = 2$, it decreases even if the radiation term is still constant. This is because the convection term decreases along x, and

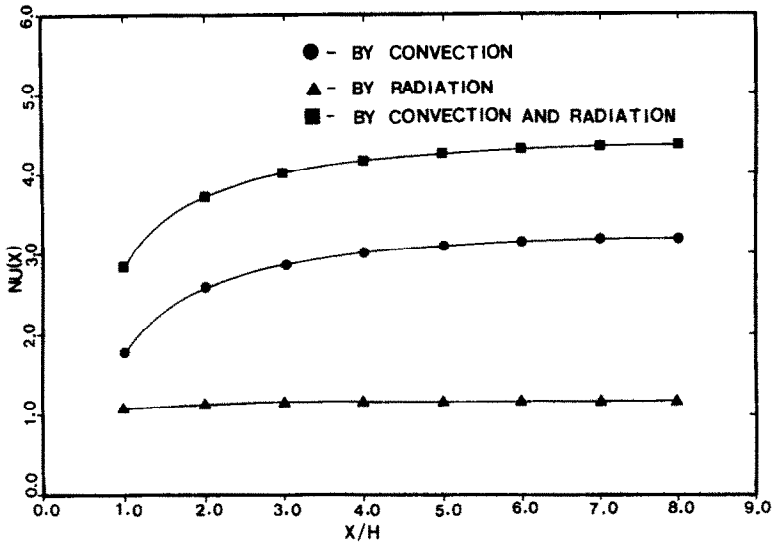

FIG. 5. Nusselt number ($Q_s = 3$).

at around $x/H = 2$ the total heat transfer is at a maximum with the radiation plus convection.

By increasing the source flux, the total heat transfer coefficient also increases as shown in Figs. 4 and 5. It is obvious that the effect of radiative transfer becomes more significant to the total heat transfer as the fluid inertia decreases. The convection heat transfer is larger than the radiation even if the source flux still increases. This is the reason that the convection heat transfer coefficient also increases with the effect of the radiative transfer, by increasing the source flux.

From the results, the heat transfer with no radiation continuously decreases along x. With low values of source flux, the heat transfer increases and at small values of x, decreases again. With high values of source flux, the heat transfer still increases with x though the rate of increase is smaller far downstream, obviously because of the increased radiative absorption from the larger source strength.

Figure 6 shows that the temperature continuously increases in the porous medium along the x-direction with the source flux of $Q_s = 3$. Temperatures increase until y/H reaches about 0.85 along the y-direction. Maximum temperatures occur around $y/H = 0.85$. Past this point, temperatures decrease because of inertia effects in the free stream region and boundary conditions at the interface, since the temperature gradients are almost equal ($\partial T^+/\partial y \approx \partial T^-/\partial y$). The maximum temperature in the porous region around $y/H = 0.85$ is approximately 1.5 times larger than the free stream temperature at $x/H = 8$.

3. EXPERIMENTAL ANALYSIS

To verify the analytical model developed, an experiment was carried out using the naphthalene sublimation technique for the case of negligible radiation field. This was conducted to study the effects of a layer of porous medium on mass transfer from a flat naphthalene surface and to invoke the heat/mass transfer analogy.

3.1. *Experimental procedure and data reduction*

A flat plate of naphthalene was cast, and a layer of rigid porous ceramic block [12] with the size of $9.7 \times 20.0 \times 1.905$ (or 1.11) cm was put on the naphthalene surface at a distance of $l = 6.5$ cm from the leading edge of the naphthalene plate as shown in Fig. 1. This assembly was placed in a once-through, low-

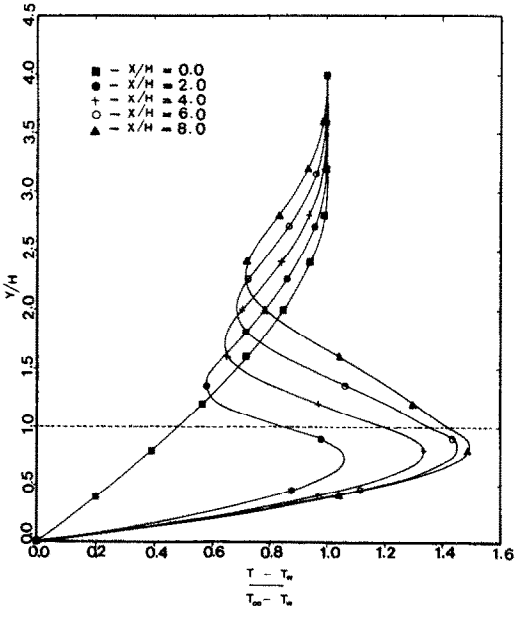

FIG. 6. Temperature profile ($Q_s = 3$).

speed wind tunnel. The size of the working area in the wind tunnel, in which the naphthalene cast on a steel plate was installed, was $20 \times 61 \times 20$ cm.

The naphthalene mold was a thick, 19×19 cm flat square, steel block with a 15×17 cm square, naphthalene surface, which was flat and smooth. In each experiment, the distribution of the local mass transfer coefficient was obtained by measuring the elevations at discrete points on the naphthalene surface before and after air was circulated through the test section. The elevations at 238 points (17 points in the spanwise direction, 14 points in the streamwise direction) were measured in a region on the naphthalene surface.

During the experiments, air was always maintained at 22 ± 1 C. The temperature of the air was measured and recorded periodically. The duration of the test run, which lasted about 2–3 h, was recorded with a watch. Supplementary experiments were also performed to determine the effect of natural convection during the elevation measurements.

The local mass transfer coefficients are determined from the measured change of the elevation (Δy) at each of the measurement points, the duration of the experiment (Δt), the density of solid naphthalene (ρ_s), and the difference between the naphthalene vapor density at the plate surface (ρ_w) and the naphthalene vapor density in the free stream (ρ_∞)

$$h_m = \frac{\dot{m}}{(\rho_w - \rho_\infty)} = \frac{\rho_s \Delta y}{(\rho_w - \rho_\infty)\Delta t} \tag{11}$$

where $\dot{m}$ is the mass transfer rate (i.e. the sublimation rate) per unit area.

From the *Chemical Engineer's Handbook* [13], data for naphthalene are $D = 0.62 \times 10^{-5}$ m^2 s^{-1}, $\rho_s = 1145$ kg m^{-3}, $M = 128.16$ kg kmol^{-1}. The naphthalene vapor density at the wall is calculated from the vapor pressure–temperature relation for naphthalene [14] in conjunction with the perfect gas law

$$\rho_w = \frac{p_{nw} M}{\bar{R} T_w} \tag{12}$$

where

$$\log_{10} p_{nw} = 11.884 - \frac{6713}{T_w}.$$

The free stream naphthalene vapor density is assumed to be effectively zero. Thus, the local mass transfer coefficient and Sherwood number are

$$h_m = \frac{\rho_s \Delta y}{\rho_w \Delta t} \tag{13}$$

$$Sh_H = \frac{h_m H}{D}. \tag{14}$$

3.2. *Measurement of permeability*

Permeability of four rigid porous ceramic blocks was measured by forcing air through the porous material, measuring the pressure drop across the porous material, and the flow rate through it [15]. The application of Darcy's law in its simplest form is

$$\frac{dp}{dx} = \frac{\mu}{K} u. \tag{15}$$

At higher flow rates, the Forchheimer equation is applicable

$$\frac{dp}{dx} = \frac{\mu}{K} u + \frac{\rho F}{\sqrt{K}} u^2. \tag{16}$$

The above equation can be written in a straight line form as follows:

$$\frac{(dp/dx)}{u} = A + Bu \tag{17}$$

where

$$A = \frac{\mu}{K}$$

$$B = \frac{\rho F}{\sqrt{K}}.$$

The number of experimental points for each of the samples was over 15. The range of the flow velocity was from about 0.02 to 0.46 m s^{-1}. The results are listed in Table 1. The curve fitting equation listed in Table 1 is $(dp/dx)/u$ vs u shown in Fig. 7. By fitting a straight line to the data, the permeability K and the constant F can be calculated from equation (17). From Fig. 7 and equation (15), the value of A should be constant if we use Darcy's law. Thus Darcy's law is not proper in our experimental range.

3.3. *Input parameters*

Three different rigid porous ceramic blocks (Samples II and IV in Table 1) were considered here. The boundary layer thickness for velocity at $x = 0.065$ m (the starting point for the theoretical input) was assumed to be equal to the height of the porous medium. The Sherwood number at the leading edge of the porous medium was assumed to be equal to the Sherwood number for the experiment. The momentum and mass equations for laminar flow were used since the total length measured for the experiment was within $x = 0.15$ m, which gives a laminar flow Reynolds number.

In each plot, four lines are shown; one is for the experimental result, another is the theoretical result, and the other two lines are results from equation (18) for laminar flow and equation (19) for turbulent flow over the flat surface without the porous medium. Both equations were used to check whether both experimental and theoretical results were reasonable. The velocity of $u = 6.5$ m s^{-1} was used in the experiment. The local Sherwood numbers based on the length scale of the porous height are

$$Sh_H = \frac{h_m H}{D} = 0.332 Re_H^{1/2} Sc^{1/3} (H/x)^{1/2} \tag{18}$$

Table 1. Experimental measurement of permeability

Sample	PPI†	Density (g cm^{-3})	Porosity‡ (%)	Velocity range (m s^{-1})	Pressure drop (N m^{-3})	Fitting equation		Permeability, K (m^2)	Constant, F
						dp/dx (N m^{-3})	$(dp/dx)/u$ (N s m^{-4})		
I	—	0.40	—	0.02–0.30	48–980	$3.18+2284u+3320u^2$	$2372+2972u$	7.67×10^{-9}	0.216
II	30	0.35	83	0.03–0.46	25–546	$9.01+562.3u+1364u^2$	$700.3+1031u$	2.60×10^{-8}	0.138
III	20	0.36	82	0.03–0.31	11–144	$3.89+216.4u+798.7u^2$	$294.8+526.2u$	6.17×10^{-8}	0.108
IV	10	0.34	84	0.02–0.45	3–124	$0.20+123.9u+341.4u^2$	$128.1+330.8u$	1.42×10^{-7}	0.103

† PPI, pores per inch.
‡ According to the data of UDICELL Ceramic Foam of Special Metals Corporation, Japan.

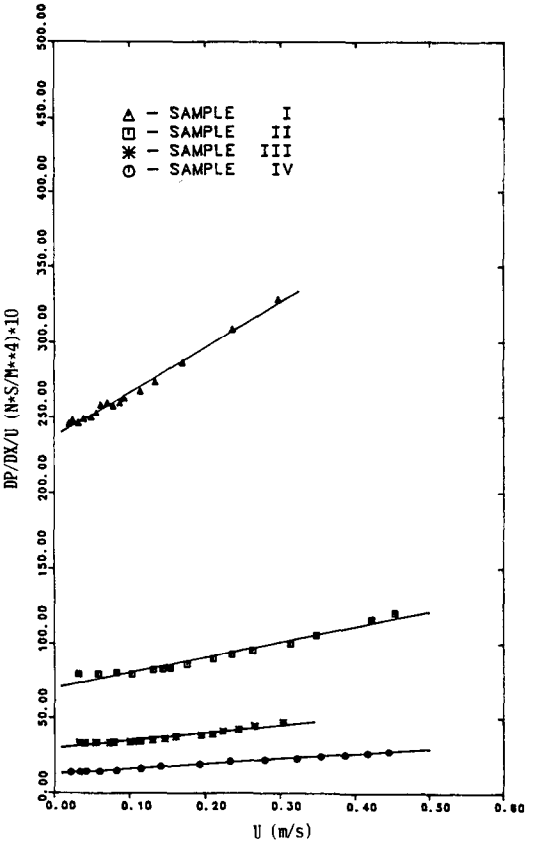

FIG. 7. Pressure drop through the porous media.

$$Sh_H = \frac{h_m H}{D} = 0.0296 Re_H^{4/5}\, Sc^{1/3} (H/x)^{1/5}. \qquad (19)$$

3.4. *Experimental and theoretical results*

Figure 8 shows that the experimental Sherwood number is very large near the leading edge of the naphthalene plate because of the developing boundary layer. The Sherwood number decreases very sharply near $x = 0.055$ m and increases very rapidly before the leading edge of the porous medium from the effects of the wake, and is maximum around $x = 0.065$ m where the porous medium is attached. Past $x = 0.065$ m, the Sherwood number decreases very sharply from the effects of the porous medium. Around $x = 0.12$ m, the Sherwood number increases again from the effects of the wake over, at the side of, and behind the porous medium. This occurs because the flow separates over, at the side of, and at the back-facing step formed by the aft end of the porous material. Both experimental and theoretical results correspond well with each other through the porous medium. The results from the above two equations (without considering the porous medium) are smaller than both the experimental and theoretical results

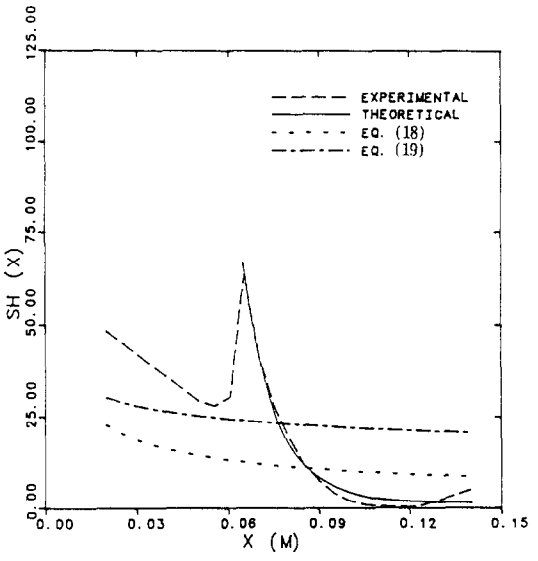

FIG. 8. A comparison of the experimental and theoretical results ($Re = 4538$, $Da = 2.1 \times 10^{-4}$, $\varepsilon = 0.83$, $Sc = 2.56$, $K = 2.6 \times 10^{-8}$ m^2, $H = 0.0111$ m).

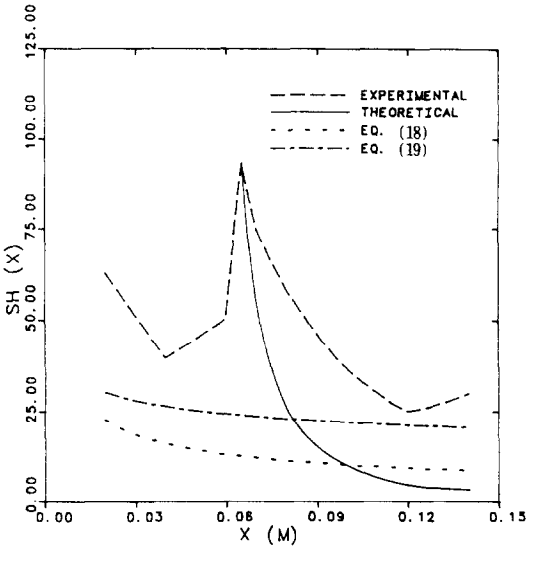

FIG. 10. A comparison of the experimental and theoretical results ($Re = 4538$, $Da = 1.2 \times 10^{-3}$, $\varepsilon = 0.84$, $Sc = 2.56$, $K = 1.4 \times 10^{-7}$ m^2, $H = 0.0111$ m).

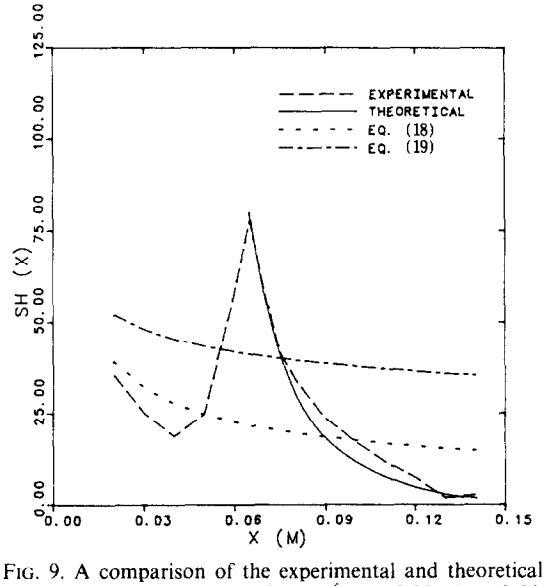

FIG. 9. A comparison of the experimental and theoretical results ($Re = 7788$, $Da = 7.2 \times 10^{-5}$, $\varepsilon = 0.83$, $Sc = 2.56$, $K = 2.6 \times 10^{-8}$ m^2, $H = 0.01905$ m).

at $x = 0.075$ m, since the developing boundary layer effects and the wake effects are larger than the porous effects within the porous medium. But past $x = 0.075$ m, the latter results are much smaller than the former results.

In Fig. 9, the characteristics of the Sherwood number show similar trends to Fig. 8. The experimental and theoretical results correspond well with each other.

Figure 10 also shows similar trends to Figs. 8 and 9 over the entire regions. Both experimental and theoretical Sherwood numbers of Fig. 10 ($Da = 1.2 \times 10^{-3}$) are larger over the entire regions than those of Fig. 8 ($Da = 2.1 \times 10^{-4}$), using the same Reynolds number of $Re = 4538$. The differences between the experimental and theoretical results are larger through the porous medium. The results from equations (18) and (19) are much smaller than those for the experiment over the entire region. Thus, at larger Darcy number both the developing effects and the wake effects greatly affect the flow preceding the porous medium. The wake effects through, over, at the side of, and at the back of the porous medium also affect greatly the flow. They apparently cause greater flow penetration at the leading edge of the porous 'step' due to the presence of a rotating vortex there, while the wake at the back of the porous block apparently causes a flow reversal that penetrates the rear of the block and causes a slight increase in the mass transfer coefficient there. These effects were not considered in the analytical mode. The Sherwood number and Reynolds number are based on the height of the porous medium.

3.5. *Heat and mass analogy*

The mass transfer results presented here may be converted to heat transfer results by employing the analogy between heat and mass transfer.

3.5.1. *Non-porous region.* According to the analogy, the conversion between the Sherwood and Nusselt number results can be accomplished by noting the relations [16]

$$Sh = Cf(Re)Sc^n \tag{20}$$

$$Nu = Cf(Re)Pr^n. \tag{21}$$

The above equations are inferred from both theoretical calculations and experimental measurements for laminar flow, and from only experimental measure-

ments for turbulent flow. The specific values of the coefficient C, the function $f(Re)$, and exponent n vary with the nature of the surface geometry and the type of the flow (laminar or turbulent), but they are independent of the nature of the fluid [17].

From the above equations, it follows that

$$Nu = (Pr/Sc)^n Sh. \quad (22)$$

The exponent n is 1/3 on the flat plate in which air is a flowing fluid and the Sherwood number would be multiplied by the ratio (0.712/2.56) with the exponent term of 1/3.

3.5.2. *Porous region.* From the conservation equations normalized by use of dimensionless variables and equations (2)–(5) within the porous region, the momentum equation is a function of not only Re but also Da and ε. The mass and energy equation are a function of the effective Schmidt and Prandtl numbers, respectively. Thus, following the same procedure as above, the Sherwood and Nusselt numbers are

$$Sh = C_s f_s(Re, Da, \varepsilon) Sc_e^{n_s} \quad (23)$$

$$Nu = C_n f_n(Re, Da, \varepsilon) Pr_e^{n_n}. \quad (24)$$

If $C_s = C_n$, $f_s = f_n$, and $n_s = n_n$, equation (22) can be applied for analogy in the porous region as in the non-porous region

$$Nu = (Pr_e/Sc_e)^n Sh. \quad (25)$$

But the relations should be first verified from the experimental measurements. These will become another good research topic.

4. CONCLUSIONS

The overall heat transfer coefficients were calculated numerically to see the effects of radiation around the porous medium put on the flat plate at a distance from the leading edge of the flat plate. To verify the analytical model developed, an experiment was carried out using the naphthalene sublimation technique for the negligible radiation fields and a comparison was made between both results in terms of the Sherwood number.

The following conclusions are obtained below.

(1) The heat transfer coefficients show that by increasing the source flux ($Q_s = 0$–3) the effects of radiative transfer become more significant to the total heat transfer because of the increased radiative absorption of the porous materials.

(2) The theoretical results correspond well with the experimental results at the smaller Darcy number ($Da = 2.1 \times 10^{-4}$–7.2×10^{-5}) and appear reasonable. But at the higher Darcy number ($Da = 1.2 \times 10^{-3}$), the experimental results are much larger than the theoretical results due to both developing boundary effects and wake effects around the porous medium. The numerical analysis did not consider these effects.

(3) The permeability of ceramic blocks used for experiment was also measured and the Forchheimer equation is applicable in our measurement range ($K = 1.42 \times 10^{-7}$–7.67×10^{-9}).

(4) If the following relation, $Nu = (Pr_e/Sc_e)^n Sh$, is verified in the porous region from the experimental measurements as in the non-porous region, the mass transfer results presented here may be converted to heat transfer results by employing the heat/mass analogy.

REFERENCES

1. W. E. Reifsnyder, Wind profiles in a small isolated forest stand, *Forest Sci.* **1**(1), 289–297 (1955).
2. O. T. Denmead, Evaporation sources and apparent diffusivities in a forest canopy, *J. Appl. Met.* **3**, 383–389 (1964).
3. R. N. Meroney, Characteristics of wind and turbulence in and above model forests, *J. Appl. Met.* **7**, 780–788 (1968).
4. T. Kawatani and R. N. Meroney, Turbulence and wind speed characteristics within a model canopy flow field, *Agric. Met.* **7**, 143–158 (1970).
5. J. C. Koh *et al.*, Friction factor for isothermal and nonisothermal flow through porous media, *J. Heat Transfer* **99**, 367–373 (1977).
6. J. T. Hong, C. L. Tien and M. Kaviany, Non-Darcian effects on vertical-plate natural convection in porous media with high porosities, *Int. J. Heat Mass Transfer* **28**, 2149–2157 (1985).
7. E. M. Sparrow and P. A. Bahrami, Experiments on natural convection from vertical parallel plates with either open or closed edges, *J. Heat Transfer* **102**, 221–227 (1980).
8. J. C. Han *et al.*, Local heat/mass transfer distribution around sharp 180 degree turn in a smooth square channel, Symp. on Transport Phenomena in Rotating Machinery, Honolulu, 28 April–3 May (1985).
9. K. B. Lee, Heat and mass transfer in highly porous media, Ph.D. Dissertation, University of Texas at Austin (1986).
10. B. E. Launder and D. B. Spalding, The numerical computation of turbulent flows, *Comput. Meth. Appl. Mech. Engng* **3**, 269–289 (1974).
11. S. Ergun, Fluid flow through packed columns, *Chem. Engng Prog.* **48**, 89–94 (1952).
12. Special Metals Corporation, UDICELL Ceramic, Japan.
13. J. H. Perry (Editor), *Chemical Engineer's Handbook*, 5th Edn, pp. 3–39. McGraw-Hill, New York (1973).
14. H. H. Sogin, Sublimation from disks to air streams flowing normal to their surfaces, *Trans. ASME* **80**, 61–69 (1958).
15. K. B. Lee and Z. Lu, Experimental determination of the permeability of a porous media, *Energy R&D* **10**(2), 57–63 (1988).
16. F. E. M. Saboya and E. M. Sparrow, Experiments on a three-row fin and tube heat exchangers, *J. Heat Transfer* **98**, 520–522 (1976).
17. F. P. Incropera and D. P. DeWitt, *Fundamentals of Heat Transfer*, p. 324. Wiley, New York (1981).

TRANSFERT DE CHALEUR ET DE MASSE THEORIQUE ET EXPERIMENTAL DANS LES MILIEUX FORTEMENT POREUX

Résumé—On calcule numériquement pour les écoulements laminaires bidimensionnels sur une plaque plane, les coefficients de transfert de chaleur et de masse autour d'un milieu poreux placé à distance du bord d'attaque. Pour vérifier le modèle analytique, on conduit une expérimentation avec la technique de sublimation du naphtalène dans le cas d'un champ radiatif négligeable. A partir des effets de sillage, le nombre de Sherwood est maximal autour de la région où le milieu poreux est attaché. Les résultats théoriques correspondent bien aux résultats expérimentaux aux petits nombres de Darcy. La perméabilité des blocs de céramique utilisés pour l'expérience est aussi mesurée et l'équation de Forchheimer est applicable dans le domaine de mesure considéré.

THEORETISCHE UND EXPERIMENTELLE UNTERSUCHUNG DES WÄRME- UND STOFFÜBERGANGS IN HOCH-PORÖSEN MEDIEN

Zusammenfassung—Die Wärme- und Stoffübergangskoeffizienten in einem porösen Medium, das in großer Entfernung von der Anströmkante auf einer ebenen Platte liegt, werden für zweidimensionale laminare Strömung numerisch berechnet. Um das entwickelte analytische Modell zu überprüfen und die Analogie zwischen Wärme- und Stoffübertragung heranzuziehen, wird für den Fall vernachlässigbarer Strahlung mit Hilfe der Naphthalin-Sublimationstechnik ein Versuch ausgeführt. Aufgrund der Nachlaufeffekte ist die Sherwood-Zahl in der Region maximal, in welcher das poröse Medium angebracht ist. Die theoretischen Ergebnisse stimmen für kleine Darcy-Zahlen gut mit experimentellen Resultaten überein. Zusätzlich wurde die Permeabilität der beim Versuch verwendeten keramischen Blöcke gemessen. In dem hier verwendeten Bereich ist die Forchheimer-Gleichung anwendbar.

ТЕОРЕТИЧЕСКОЕ И ЭКСПЕРИМЕНТАЛЬНОЕ ИССЛЕДОВАНИЕ ТЕПЛО- И МАССОПЕРЕНОСА В ВЫСОКОПОРИСТЫХ СРЕДАХ

Аннотация—Численно рассчитываются коэффициенты тепло- и массопереноса вблизи пористой среды, расположенной на плоской пластине вдали от ее передней кромки, в случае двумерных ламинарных течений. С целью проверки адекватности разработанной теоретической модели и установления аналогии между тепло- и массопереносом проводится эксперимент по сублимации нафталина. Благодаря эффектам следа число Шервуда достигает максимума на участке, где находится пористая среда. Теоретические результаты хорошо согласуются с экспериментальными данными при малом числе Дарси. Измеряется проницаемость используемых в эксперименте керамических блоков, и найдено, что в пределах данной области измерений применимо уравнение Форшхаймера.